Simulation of crystal and liquid potassium via restricted path-integral molecular dynamics

Ki-Dong Oh
Department of Physics, University of Arizona, Tucson, Arizona 85721

P. A. Deymier
Department of Materials Science and Engineering, University of Arizona, Tucson, Arizona 85721
(Received 27 October 1998)

The path-integral molecular-dynamics method is employed to study the effect of temperature on a simple metal (potassium) model system. The simple metal undergoes a phase transformation upon heating. Calculated dynamic properties indicate that the atomic motion changes from a vibrational to a diffusive character identifying the transformation as melting. Calculated structural properties further confirm the transformation. Ionic vibrations in the crystal state and the loss of long-range order during melting modify the electronic structure and in particular localize the electrons inside and at the border of the ion core. [S0163-1829(99)00117-4]

I. INTRODUCTION

The goal of the present work is to predict the equilibrium and dynamical properties of systems with strongly coupled electronic and ionic degrees of freedom. Of particular interest is the interplay between electronic and atomic structure during a phase transformation. In this paper, we present the application of a recently developed first-principle numerical method: the path-integral molecular-dynamics (PIMD) method[1,2] to the study of an alkali metal, namely, potassium (K). The choice of this system is essentially driven by its simplicity but also by the availability of experimental data such as structural and thermodynamic properties in both liquid and solid phases as well as vibrational properties for the crystal.[3–5] Although the alkali metals are often considered simple nearly free-electron systems (with only one single valence electron per atom), they possess physical properties that make them good prototype systems with relevance to many current issues in materials science. Some of these properties include (1) metal to nonmetal transitions (M/NM), the M/NM transition in expended molten alkali metals[6,7] remains an outstanding many-body problem of strongly correlated systems at high temperature; (2) immiscibility, while most binary alloys of alkali metals show miscibility, the K-Li and Na-Li exhibit a miscibility gap;[8] (3) structural phase transformations, the body-centered-cubic Na and Li crystals exhibit a martensitic transition at low temperature[4] but one of the most obvious and common transformations is that from the solid phase to liquid phase, namely, melting.

While melting of numerous materials has been extensively investigated by classical molecular dynamics using empirical pair or many-body potentials, there have been few first-principles investigations of this ubiquitous phenomenon. The coupling between the structure of the solid/liquid and the electronic structure necessitates a theoretical approach based on first principles. The method to be used should also allow for the calculation of properties at finite temperatures such as dynamical and thermodynamic properties.

In the field of *ab initio* molecular dynamics (MD), the method of Car and Parrinello,[9] based on the density-functional theory (DFT) has enjoyed a great popularity over recent years. DFTMD has been employed to investigate a very large number of problems from condensed matter to chemistry to biology.[10] In contrast, applications of molecular-dynamics simulations using the discretized path-integral (PI) representation[11] of quantum particles have been limited mostly to the simulation of systems containing a small number of quantum degrees of freedom (such as in the solvation of a single quantum particle in a classical fluid[12]) or to problems where quantum exchange is not dominant.[13] Progress in the simulation of fermionic systems by the path-integral Monte Carlo method[14–17] have opened the way toward the implementation of a path-integral-based finite-temperature *ab initio* molecular-dynamics method. The PIMD method has demonstrated recently its potency in the simulation of degenerate electron plasma and liquid potassium.[1,2] This method uses the discretized path-integral representation of quantum particles as a starting point, and introduces a restricted form of the path that accounts for Fermi statistics. This scheme is then coupled to classical molecular-dynamics equations of motion for sampling the configurational space of the electronic and ionic degrees of freedom. This method is capable of modeling electronic systems beyond the Hartree-Fock approximation.[1,2] Furthermore, since the PIMD method is based on a position representation of the quantum states, it appears to be well suited to simulating systems which electronic structure may change from delocalized to more localized electrons.

We show in this paper that the PIMD successfully models the body-centered-cubic crystal structure of potassium metal at low temperature. Upon increasing the temperature, the metal transforms to a liquid. The predicted melting temperature is below the experimental value. This deviation is assigned to a short-range approximate potential used in place of the usual long-range Coulomb potential in order to reduce computational cost. The phase transformation is characterized thermodynamically via energies, structurally via pair-distribution functions as well as dynamically via the mean-square displacement and the vibrational power spectrum. Vibrations in the crystal appear to induce some localization in the electron density. As melting takes place, the electronic

structure responds to the loss of long-range order in the atomic structure by additional localization.

This paper is organized as follows. In Sec. II, we briefly review the method of PIMD as well as its practical implementation and application to the simulation of alkali metals. Results are reported in Sec. III. In Sec. IV, we draw some conclusions concerning the applicability of the PIMD method to some other systems.

II. METHOD AND MODEL

In this section we briefly review the PIMD method[1,2] and provide some details concerning its implementation for the simulation of alkali metals. The PIMD method makes use of (a) the discretized path-integral representation of quantum particles as closed ''polymeric'' chains of classical particles (beads) coupled through harmonic springs,[18] (b) the treatment of quantum exchange as crosslinking of the chains,[18] (c) the nonlocality of crosslinking (exchange) along the chains (in imaginary time),[14] (d) the restricted path integral[15,16,19] to resolve the problem of negative weights to the partition function resulting from the crosslinking of even numbers of quantum particles.

Since, the main difficulty in the PIMD method resides in the treatment of the electronic degrees of freedom we first develop the formalism in the case of a system of electrons. We subsequently add the ionic degrees of freedom to the model for the electron system. The partition function of a system of N quantum particles expressed in a position representation takes the form[20]

$$Z=\int dR_1\rho(R_1,R_1;\beta)=\int \prod_{n=1}^{P} dR_n \prod_{n=1}^{P} {}^{*}\rho(R_n,R_{n+1};\varepsilon), \tag{1}$$

where ρ is the density matrix, $R=\{\mathbf{r}^{(1)},\ldots,\mathbf{r}^{(N)}\}$ stands for the position of the particles, and $\beta=1/kT$. In Eq. (1), we have used the convolution property of the density matrix and introduced $(P-1)$ intermediate states. The * in the product indicates the cyclic condition $R_{P+1}=R_1$ and $\varepsilon=\beta/P$. Since the wave function of fermions is antisymmetric, the density matrix can be positive or negative and convergence is slow. However, the diagonal density matrix can be evaluated by restricting paths to remain in the region of phase space where their sign is positive.[15,16,19] With this restriction, Eq. (1) is exact, but since one does not know the exact density matrix, it is necessary to replace it by some reasonable approximation. The nodes of the approximate density matrix (loci of points where the density matrix is zero) should be as close as possible to those of the exact density matrix if one hopes to calculate accurate properties. If P is sufficiently large, we can use Trotter's approximation to separate the kinetic and the potential contributions to the density matrix.[21]

The propagator, $\rho(R_n,R_{n+1};\varepsilon)$, is approximated for small ε using the Trotter formula[21] by

$$\begin{aligned}\rho(R_n,R_{n+1};\varepsilon)&=\langle R_n|\exp(-\varepsilon H_{\mathrm{op}})|R_{n+1}\rangle\\ &\approx\int dR\langle R_n|\exp(-\varepsilon T_{\mathrm{op}})|R\rangle\\ &\quad\times\langle R|\exp(-\varepsilon V_{\mathrm{op}})|R_{n+1}\rangle,\end{aligned} \tag{2}$$

where the Hamiltonian operator H_{op} is decomposed into the kinetic operator T_{op} and the potential operator V_{op}. For a local potential operator, ρ becomes

$$\rho(R_n,R_{n+1};\varepsilon)\approx\langle R_n|\exp(-\varepsilon T_{\mathrm{op}})|R_{n+1}\rangle\exp[-\varepsilon V(R_{n+1})], \tag{3}$$

where $V(R_{n+1})$ is a potential function of the position. This potential function may describe any potential field in which the electrons evolve including electron-electron Coulomb interactions or electron-ion interactions.

For the kinetic matrix, we use the exact noninteracting density matrix:

$$\begin{aligned}\rho_{NI}(R_n,R_{n+1};\varepsilon)&=\langle R_n|\exp(-\varepsilon T)|R_{n+1}\rangle\\ &=\left[\frac{m}{2\pi\varepsilon\hbar^2}\right]^{3N/2}\det[A_{n,n+1}]\end{aligned} \tag{4}$$

with $[A_{n,n+1}]$ representing a $N\times N$ matrix in which elements are expressed as $A^{ij}_{n,n+1}=e^{-\beta(m/2\beta\varepsilon\hbar^2)(r_n^{(i)}-r_{n+1}^{(j)})^2}$. In the preceding relation, the indices i and j label the electrons. The expression for the density matrix of Eq. (4) is given in a position representation. It is obtained by using a complete set of states represented by Slater determinants of plane waves. The use of a position representation has the advantage over methods employing only a finite basis set of providing a better description of electronic orbitals that may change form qualitatively. This property makes the path-integral formalism particularly suited for systems with electrons going from localized to delocalized orbitals. At this stage, however, since Slater determinants of plane waves are solutions to the Hartree-Fock equation for free electrons, the noninteracting density matrix does not describe electron correlation. Although the noninteracting density matrix does not describe electron correlation, in the limit of high temperature, its nodes approximate reasonably well those of the exact density matrix.[15]

We now construct an approximate form for the density matrix that includes electron correlation. The determinant of the kinetic matrix in the absence of quantum exchange is factored out of Eq. (4):

$$\det[A_{n,n+1}]=\prod_{i=1}^{N} A^{ii}_{n,n+1}\det[E_{n,n+1}], \tag{5}$$

where all the exchange effects (including the sign of the density matrix) are included in $[E]$ where the elements are defined as $E^{ij}_{n,n+1}=A^{ij}_{n,n+1}/A^{ii}_{n,n+1}$. In the limit of $\varepsilon\to 0$, the matrix $[E]$ reduces to the identity matrix and the system collapses into a bosonic state. To prevent this undesirable behavior, following Hall, we recast Eq. (5) in a nonlocal form:[14]

$$\det[A_{n,n+1}]\to\prod_{i=1}^{N} A^{ii}_{n,n+1}\prod_{m=1}^{P}(\det[E_{n,m}])^{1/P}. \tag{6}$$

Such a nonlocal form for the density matrix cannot be obtained from simple Slater determinants of plane waves. Equation (6) should, therefore, represent electrons beyond the Hartree-Fock approximation. A nonlocal density matrix would, therefore, account for some electron correlation. This approximation was shown to model a semidegenerate elec-

tron plasma near metal density beyond the Hartree-Fock approximation.[1,2] In this work, the calculated kinetic and potential energies did not correspond to the Hartree-Fock values but approached the values for a fully correlated plasma.

With the restricted path integral, the integrand of the partition function is positive and Z can now be rewritten in a classical form usable with a molecular-dynamics (MD) scheme:

$$Z=\int \prod_{n=1}^{P} dR_n \exp[-\beta V_{\mathrm{eff}}(R_1,\ldots,R_P)], \tag{7}$$

where the effective potential includes quantum exchange and correlation. For systems containing electrons with nonidentical spins, the density matrix is approximated as the product of two determinants taking the form of Eq. (6); one determinant for the electrons with one type of spin and another determinant for the electrons with the other type of spin.[22] Therefore, in the case of a nonpolarized fermion system with N_{el} electrons, a microcanonical ensemble sampling of the quantum states of the system can now be performed by solving for the trajectories generated by the classical Hamiltonian:

$$\begin{aligned} H=&\sum_{k=1}^{N_{\mathrm{el}}}\sum_{i=1}^{P}\frac{1}{2}m^*(\dot{r}_i^{(k)})^2+\sum_{i=1}^{P}\sum_{k>l}^{N_{\mathrm{el}}}\sum_{l=1}^{N_{\mathrm{el}}-1}\frac{(-e)(-e/P)}{4\pi\varepsilon_0|r_i^{(k)}-r_i^{(l)}|}\\ &+\sum_{k=1}^{N_{\mathrm{el}}}\sum_{i=1}^{P}{}^{*}\frac{m_eP}{2\hbar^2\beta^2}(r_i^{(k)}-r_{i+1}^{(k)})^2\\ &-\frac{1}{\beta}\sum_{s=\uparrow}^{\downarrow}\frac{\sum_{i=1}^{P}\sum_{j=1}^{P}\ln\det[E_{ij}]_s\theta_{ijs}^{+}}{\sum_{i=1}^{P}\sum_{j=1}^{P}\theta_{ijs}^{+}}. \end{aligned} \tag{8}$$

Here, m^* is some arbitrary mass (we chose $m^*=1$ a.m.u,) used to define an artificial kinetic energy for the quantum states in order to explore the effective potential surface, V_{eff} constituted of the last three terms in Eq. (8). The fourth term is an effective exchange potential for the electrons with spin up ($s=\uparrow$) and spin down ($s=\downarrow$). The function θ_{ij}^{+} ensures the path restriction by taking on the values 1 and 0 for paths with positive and negative $\det[E]$, respectively. In Eq. (8), the second term accounts for the electron/electron Coulomb interactions. The forces derived from the exchange potential are calculated as means over the paths with positive determinant. Therefore, an effective force calculation requires a satisfactory sample of such paths. Since the exchange potential offers a barrier to paths with negative determinants, it biases the sampling of phase space toward configurations with positive determinants. Although many configurations with negative determinants exist and evolve, they do not contribute to the exchange forces.

Extension of the restricted-PIMD method to include the classical ionic degrees of freedom is straightforward provided the electrons interact with the ions via local pseudopotentials. In this case the Hamiltonian becomes

$$\begin{aligned} H=&\sum_{k=1}^{N_{\mathrm{el}}}\sum_{i=1}^{P}\frac{1}{2}m^*(\dot{r}_i^{(k)})^2+\sum_{I=1}^{N_{\mathrm{ion}}}\frac{1}{2}M_I\dot{R}_I^2\\ &+\sum_{I>J}^{N_{\mathrm{ion}}}\sum_{I=1}^{N_{\mathrm{ion}}-1}\Phi_{IJ}(R_{IJ})+\sum_{i=1}^{P}\sum_{k>l}^{N_{\mathrm{el}}}\sum_{l=1}^{N_{\mathrm{el}}-1}\frac{(-e)(-e/P)}{4\pi\varepsilon_0|r_i^{(k)}-r_i^{(l)}|}\\ &+\sum_{i=1}^{P}\sum_{k=1}^{N_{\mathrm{el}}}\sum_{I=1}^{N_{\mathrm{ion}}}\frac{V_{\mathrm{pseudo}}(R_I-r_i^{(k)})}{P}\\ &+\sum_{k=1}^{N_{\mathrm{el}}}\sum_{i=1}^{P}{}^{*}\frac{m_eP}{2\hbar^2\beta^2}(r_i^{(k)}-r_{i+1}^{(k)})^2\\ &-\frac{1}{\beta}\sum_{s=\uparrow}^{\downarrow}\frac{\sum_{i=1}^{P}\sum_{j=1}^{P}{}^{*}\ln\det[E_{ij}]_s\theta_{ijs}^{+}}{\sum_{i=1}^{P}\sum_{j=1}^{P}{}^{*}\theta_{ijs}^{+}}. \end{aligned} \tag{9}$$

The differences between Hamiltonian (8) and (9) include a kinetic energy for the ionic degrees of freedom as well as the ion/ion Φ_{IJ} and ion/electron V_{pseudo} interaction potentials.

We simulate crystalline and liquid potassium metal with the method of PIMD. We have chosen potassium because (1) it is a prototype free-electron metal which has been studied previously by semiempirical pair potentials, (2) there exist experimental data for the pair-correlation function of the liquid state,[3] thermodynamic,[4] and vibrational properties.[5] The simulation cell contains $54\,K^+$ and 54 nonpolarized electrons. The number of electrons with spin up and spin down is $N_{s=\uparrow}=27$ and $N_{s=\downarrow}=27$, respectively. In the crystal structure, the potassium ions and electrons are arranged on a body-centered-cubic (bcc) lattice. Electrons (necklaces) with spin up are placed on the lattice with nearest neighbors of opposite spin. Every simulation reported starts with a different initial necklace configuration obtained from randomly generated-bead positions in every electron chain. The initial bead-bead distance is chosen according to the temperature. However, in order to reduce the time for the system to reach equilibrium from its initial configuration, we have taken some care as to construct necklace initial configurations (i.e., necklace spatial extent) closely related to the anticipated equilibrium state.

As temperature is varied, the dimensions of the cell are adjusted to match the experimental density of the K crystal, this over the entire range of temperature studied. Unexpectedly, our simulations have shown that the potassium model system melts at a temperature below the experimental value of the melting point, thus the density of the liquid system reported below conforms to the value of the density of the crystal at the corresponding temperature.

Periodic boundary conditions (PBC's) are applied to the simulation cell. The numerical treatment of the electrons with PBC's is done in a fashion similar to that of some previous work on the electron plasmas.[1,2] With PBC's the system is constituted of a simulation cell and 26 image cells. Under these conditions the matrix $[E_{n,m}]$ for each spin should be a $(27N_s\times 27N_s)$ matrix. When expanded over the possible exchange cycles (exchange between two electrons, exchange among three particles, etc.), the determinant of this matrix may be written in the form

$$\det[E_{n,m}]=1-\sum_{p=1}^{27}\sum_{q=1}^{27}\sum_{i=1}^{N_s}\sum_{j=1}^{N_s}\exp\left[-\beta\frac{m}{2\beta\varepsilon\hbar^2}[(\mathbf{r}_n^{(i,q)}-\mathbf{r}_m^{(j,p)})^2+(\mathbf{r}_n^{(j,p)}-\mathbf{r}_m^{(i,q)})^2-(\mathbf{r}_n^{(i,q)}-\mathbf{r}_m^{(i,q)})^2-(\mathbf{r}_n^{(j,p)}-\mathbf{r}_m^{(j,p)})^2]\right]$$
$$+\sum_{p=1}^{27}\sum_{q=1}^{27}\sum_{r=1}^{27}\sum_{i=1}^{N_s}\sum_{j=1}^{N_s}\sum_{k=1}^{N_s}\exp\left[-\beta\frac{m}{2\beta\varepsilon\hbar^2}[(\mathbf{r}_n^{(i,q)}-\mathbf{r}_m^{(j,p)})^2+(\mathbf{r}_n^{(j,p)}-\mathbf{r}_m^{(k,r)})^2+(\mathbf{r}_n^{(k,r)}-\mathbf{r}_m^{(i,q)})^2$$
$$-(\mathbf{r}_n^{(i,q)}-\mathbf{r}_m^{(i,q)})^2-(\mathbf{r}_n^{(j,p)}-\mathbf{r}_m^{(j,p)})^2-(\mathbf{r}_n^{(k,r)}-\mathbf{r}_m^{(k,r)})^2]\right]-\cdots. \tag{10}$$

The second term in the previous equation corresponds to a sum over exchanges between pairs of electrons in the simulation cell and image cells, while the third term corresponds to exchange among three electrons, etc. The indices p, q, and r are used to specify the periodic cells including the simulation cell.

In order to make the calculation more tractable, we approximate the matrix, $[E_{n,m}]$, by a block diagonal matrix containing two blocks. This approximation is equivalent to dividing the periodic system into a physical region R containing N_s electrons isolated from (actually, weakly coupled to) its surrounding (defined as the rest of the universe). The first block in the density matrix, $[F_{n,m}]$, is a $N_s\times N_s$ matrix where the elements minimize the quantity:

$$|(\mathbf{r}_n^{(i,q)}-\mathbf{r}_m^{(j,p)})^2+(\mathbf{r}_n^{(j,p)}-\mathbf{r}_m^{(i,q)})^2-(\mathbf{r}_n^{(i,q)}-\mathbf{r}_m^{(i,q)})^2$$
$$-(\mathbf{r}_n^{(j,p)}-\mathbf{r}_m^{(j,p)2})|$$

among the possible combinations of exchange between a particle i in the simulation cell (as defined by q), and a particle j in all other cells, $p=1,27$. This procedure identifies the leading pair exchange terms in $\det[E_{n,m}]$ involving at least one particle in the simulation cell. In other words, the block, $[F_{n,m}]$, contains elements of the density matrix which corresponds to those states in the region R, maximizing the Boltzman weight of the two-cycle exchange. The second block includes the contribution of the rest of the universe to the density matrix. It contains the contribution of exchange between electrons in the image cells and a minor contribution (or zero contribution if the region R is completely isolated from the surrounding) from exchange processes between electrons in the simulation cells and all other cells. Denoting by C the determinant of the second block and provided that the assumption of isolation holds, one has, $\det[E_{n,m}]\approx C\det[F_{n,m}]$. When calculating the leading contributions to the exchange force on the electrons inside the simulation cell, as the derivative of the exchange potential of Eq. (8), the quantity C drops out and does not need to be evaluated. This approximation is valid when the electrons are fairly well localized and in particular for systems in which the electrons have a strong repulsive interaction that prevents the close approach of more than a very few electrons at a time. With this approximation, the algorithm scales as $P^2N_s^3$.

In the model, the ions K^+ are dealt with in a purely classical manner and interact through a Born-Mayer potential

$$\Phi_{IJ}(r)=\frac{Z_IZ_Je^2}{4\pi\varepsilon_0 r}+A_{IJ}e^{-r/\rho_{IJ}} \tag{11}$$

and the parameters of the potential are those fixed by Sangster and Atwood.[23] As to the electron/ion interaction, we have used a simple empty core local pseudopotential

$$V_{\text{pseudo}}(r)=\frac{-Z_Ie^2}{r},\quad r\geqslant R_c;\ \text{and}\ \frac{-Z_Ie^2}{R_c},\quad r<R_c \tag{12}$$

with a core radius $R_c=2.22$ Å.[24]

To optimize the calculation of the long-range Coulomb energy and forces, we do not use the Ewald summation but simply replace the long-range Coulomb potential in Eqs. (8) and (9) by a shorter range effective potential of the form $1/r\rightarrow 1/r\ \text{erfc}(\eta r)$ where $\eta=5.741/L_0$ and $L_0=16$ Å. erfc stands for the complementary error function. This shorter range potential is then truncated at half the size of the edge of the simulation box.

The physical potassium ion mass is $M_I=71\,830m_e$, leading to an extreme disparity in electronic and ionic time scales. For practical reasons, we use a ratio of the ion mass, M_I, to the electron bead artificial mass, m^*, of 39.1:1. The dynamics of the electrons is still significantly faster than the dynamics of the ions. We solve the equation of motion with a leapfrog scheme and an integration time step of $\sim 2.8\times 10^{-16}$ s. Most simulations were run for a minimum of 70 000 time steps or 20 ps. In some cases for the calculation of vibrational properties, we have run simulations up to 120 000 steps.

Because of the large computational cost of the calculation of the exchange effective potential and forces, the exchange forces are calculated and updated every 10 MD time steps. The values for the exchange forces are used subsequently during the 10 steps following their calculation. The chosen time step is small enough to resolve the high-frequency oscillations of the harmonic springs. In the case of systems with large P, the strong electron bead-to-bead harmonic forces of Eq. (9) may lead to nonergodic behaviors.[25] This problem can be alleviated by rescaling temperature with a chain of Nosé-Hoover thermostats.[13,26] This rescaling would ensure convergence to the right canonical distribution. We have chosen to rescale the temperature of each chain of P beads independently of each other via a simple momentum rescaling thermostat.[27] With this procedure we do not obtain a true canonical distribution, but most thermal averages will be accurate to orders N^{-1}.[28] We have also verified that with this approach over the length of our simulations the chains would sample a large region of configuration space and therefore resolve not only the fast but also the slow dynamical scale.

We have studied the potassium model system at temperatures in the interval (10–298 K). The simulation of the electronic degrees of freedom as discrete necklaces at these low temperatures would necessitate a large number of beads for convergence with respect to P. In two previous publications,[1,2] we have shown that in the study of an electron plasma at high electronic density (near the metal density of potassium), the electron system conserves a nearly degenerate character up to a temperature of 2300 K. Since temperature does not affect significantly the electronic states at the metal density, we have thermally decoupled the classical ionic degrees of freedom and the quantum electronic degrees of freedom. The electronic necklaces are attached to a thermostat set at a temperature of 1300 K, while the ionic temperature is adjusted independently with another thermostat. At the electron temperature of 1300 K, it is sufficient to employ a reasonably small number of beads for convergence of the algorithm.

We calculate the kinetic energy with the usual energy estimator derived from $\partial \ln Z/\partial\beta$.[12] Hall has shown that the exchange potential does not contribute directly to the actual energy estimator but indirectly through the equilibrium configuration.[14] With this estimator, the kinetic energy is given as a small quantity, the difference between two larger quantities, with a variance growing with P. This estimator, therefore, introduces an error on the calculated values of the average kinetic energy. We have estimated this error by calculating the standard deviation on the running cumulative average over the last 30 000 time steps of the simulations. This error is estimated to be on the order of 0.01 eV per electron.

III. RESULTS AND DISCUSSION

In a first stage, we have investigated the convergence of the algorithm with respect to the number of beads in the electron necklaces, namely, P. For this we have calculated the electron kinetic energy at an ion temperature of 273 K for systems with varying values of P. It is important to note again that each simulation starts from different initial necklace configurations. Figure 1 presents the results of these calculations. It is clearly seen that the electron kinetic energy converges to an asymptotic value of approximately 1.23 eV/electron. The algorithm appears to have nearly converged for number of beads exceeding 240. As a trade-off between accuracy and efficiency, we have chosen $P=260$ for all subsequent simulations.

The total energy of the potassium system as a function of temperature is reported in Fig. 2. The energy shows two regions separated by an apparent discontinuity of approximately 0.025 eV/atom. In Fig. 2, we have also drawn as a guide for the eyes best second-order and first-order polynomial fits to the low-temperature and high-temperature energies, respectively. The slope of the fitted curves increases from the low- to the high-temperature region indicative of larger energy fluctuations in the high-temperature systems. The dotted line in the low-temperature region is constructed from the experimental value of the constant pressure heat capacity with the constraint that it gives the calculated energy at 76 K. In view of the error on the energy, the simulated metal is in reasonable agreement with its experimental counterpart.

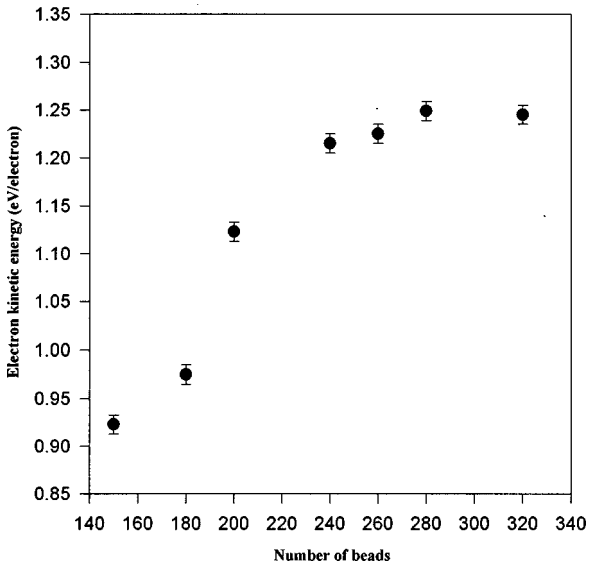

FIG. 1. Electron kinetic energy as a function of the number of necklace beads P. The ion temperature is 273 K and the electron temperature is 1300 K.

We recall that the density of the simulated potassium system varies continuously as a function of temperature as it is set to the temperature-dependent density of the solid. Therefore, the discontinuity is not associated with any discontinuous change in the volume of the system but can only result from a structural transformation. This structural transformation takes place around 210 K. As we will see later from structural data, this is a solid to liquid transformation. The calculated transformation, therefore, underestimates the melting point by nearly 120 K as potassium melts at 333 K under atmospheric pressure. This difference cannot be assigned to the fact that the density of the simulated system is constrained since such a constraint should have the opposite effect of raising the melting point. The difference between

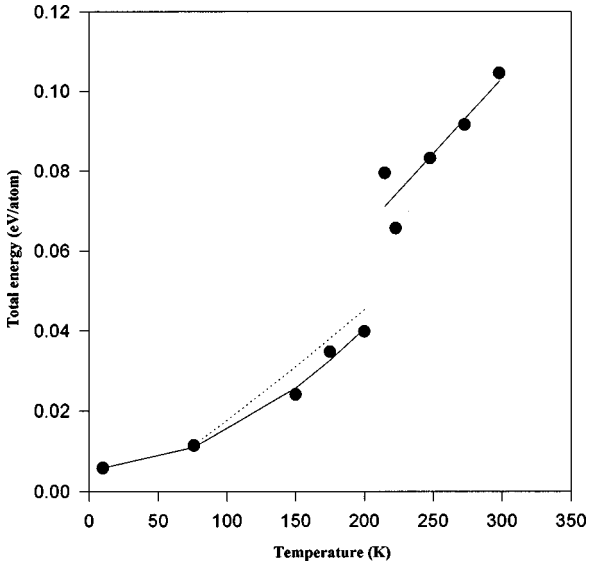

FIG. 2. Total energy versus temperature. The solid lines are fits to the data in the low- and high-temperature regions. The dotted line is constructed from the experimental constant pressure heat capacity such that it intersects the calculated energy at 76 K.

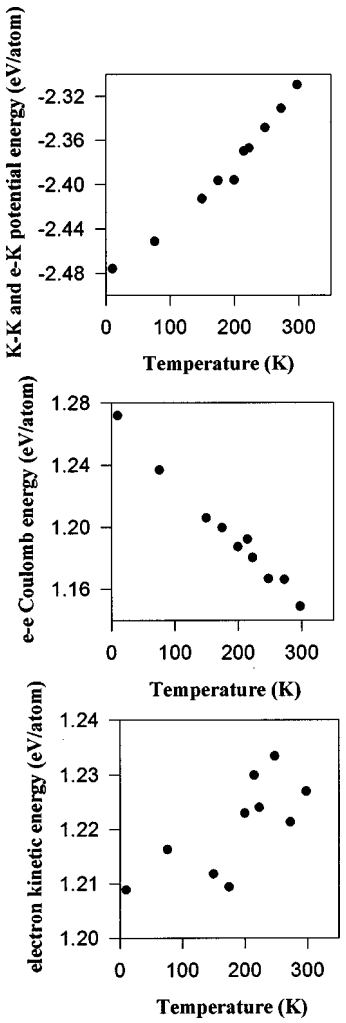

FIG. 3. Various contributions to the total energy of the potassium system as functions of temperature.

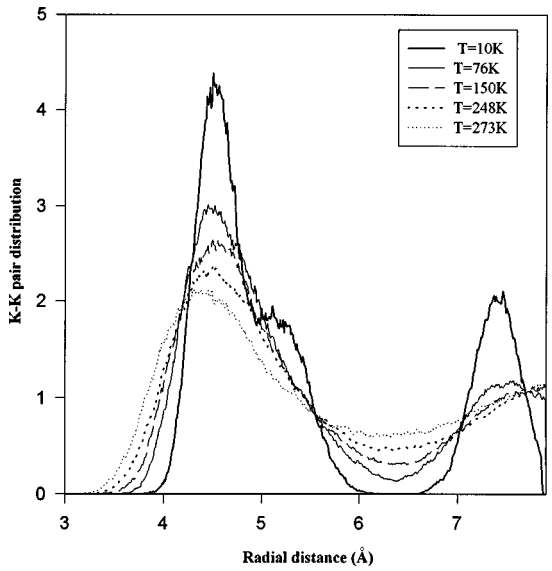

FIG. 4. Ion pair-distribution functions at the temperatures of 10 K (thick solid line), 76 K (thin solid line), 150 K (dashed line), 248 K (thick dotted line), and 273 K (thin dotted line).

experimental and simulation melting point can only result from the computer model that underestimates the strength of the K-K bond and in particular we believe that it is a consequence in part of the approximation made to reduce the range of the Coulomb interaction. In that respect it is predominantly a size effect.

To gain further insight into the energetics of the transformation, we have graphed in Fig. 3 some of the contributions to the energy of the system. The only energy that is not plotted is the classical kinetic energy of the ions. Since the temperature of the ions is maintained constant by a thermostat, the ion kinetic energy is a simple linear function of temperature and cannot account for the discontinuity in the total energy. Apart from an isolated point at 200 K, the potential energies vary reasonably continuously with temperature. In contrast, it appears that the electron kinetic energy data is separable in two groups, namely, a low-temperature group and a high-temperature group. Since the electrons in the potassium system are nearly degenerate, their kinetic energy should not be temperature dependent provided the atomic structure remains the same. Within each group the kinetic energy does not show any systematic variation. We should remember that the standard deviation on the electron kinetic energy is approximately 0.01 eV/electron. The difference between the energies of the two groups amounts to approximately 0.015–0.02 eV electron and appears to be a significant contribution to the total-energy discontinuity. The rise in kinetic energy as one crosses the discontinuity from the low-temperature to the high temperature is indicative of a change to an electronic state of higher localization in the high-temperature metal. This observation is consistent with the expected behavior of electrons in a liquid structure in contrast to a crystalline solid. As the structure disorders from crystalline to liquid, one anticipates a narrowing of the electronic band. However, since the short-range local atomic environment does not change drastically between the liquid and the solid above and below the transformation temperature, the extent of the electronic localization should be small.

We characterize the atomic structure of the simulated system via the K-K pair-distribution function. The distributions calculated at several temperatures are drawn in Fig. 4. The very low-temperature ion pair-distribution function shows a first nearest-neighbor peak at approximately 4.6 Å and a well-defined second-nearest shoulder at 5.2 Å. This second distance represents the lattice parameter of the crystal phase. The third-nearest-neighbor peak occurs near 7.4 Å. These features are characteristic of the body-centered-cubic structure of crystalline potassium. As temperature increases, the second-nearest-neighbor shoulder fades away and merges with the first-nearest-neighbor peak forming a broad asymmetric peak because of the larger amplitude of atomic motion. At the temperature of 76 K, the third-nearest-neighbor peak retains its identity. At 150 K, this peak consists only of a vague shoulder part of a much broader peak that should encompass higher-order nearest neighbors. However, due to the size of our simulation cell, we cannot resolve with much confidence the pair-distribution function beyond one half the length of the edge of the simulation cell. On the same figure, we have also plotted the K-K pair-distribution functions at the temperatures of 248 and 273 K. We have not represented the distribution at 298 K since it is practically identical to the one at 273 K. The maximum of the first-nearest-neighbor

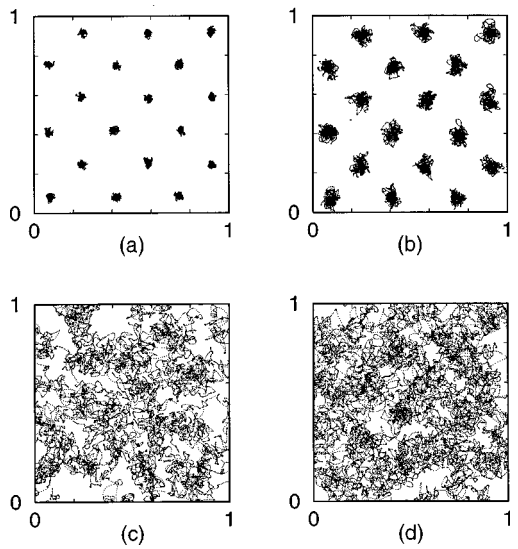

FIG. 5. Trajectories of the K ions at (a) $T=10$ K, (b) $T=76$ K, (c) $T=248$ K, and (d) $T=298$ K.

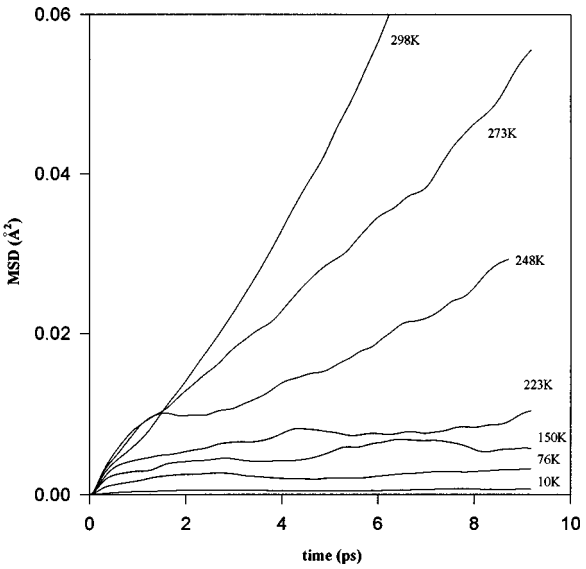

FIG. 6. Mean-square displacement (MSD) as a function of time and temperature.

peak shifts toward lower values as temperature increases. At 273 K, this maximum occurs at a distance of approximately 4.3 Å. This distance is an underestimation of the experimental K-K first-nearest-neighbor distance[3] but the calculated liquid distribution is in good qualitative accord with available experimental data.

To supplement the structural information provided by the ion pair-distribution functions, we report in Fig. 5 two-dimensional projections of the trajectories of the K ions at several temperatures. Figures 5(a) and 5(b) correspond to the crystalline state. The ionic species vibrate about clearly well-defined equilibrium lattice positions. At the two high temperatures, Figs. 5(c) and 5(d), one cannot identify lattice positions anymore. Although one may still identify some vibrational component to the ionic motion in the form of some localization in the trajectories, ionic motion is not predominantly oscillatory but also possesses a diffusive character.

More quantitative information concerning ionic motion is available from the analysis of the mean-square displacement. Figure 6 shows the mean-square displacement (MSD) of K ions as a function of time and temperature. In terms of the MSD, diffusive motion is identified by linear variation with time in the limit of large time.[29] Vibrational motion is characterized by a time-independent MSD. At the three lowest temperatures (10, 76, and 150 K), the MSD indicates that ionic motion is vibrational. At the highest temperatures of 248, 273, and 298 K, the ions exhibit diffusive motion. It is somewhat more difficult with the present data to identify on the basis of the MSD only the nature of atomic motion at the temperature of 223 K. However, because the density of the system is constrained to conform to that of the solid, it is not surprising that at 223 K, atoms in this liquid may display essentially vibrational motion.

Further information on the ionic motion is obtained from the calculation of the normalized velocity autocorrelation function (NVAF).[29] We also consider the power spectrum of the NVAF, defined as its Fourier transform. The NAVF's and the associated power spectra have to be analyzed in a qualitative manner because the time over which they are calculated is not long enough for quantitative characterization. In Fig. 7, the NVAF's at the two high temperatures of 273 and 298 K show features of the crystalline state (10 K), with oscillations representative of thermally excited phonons in crystal lattices. The contrast in ionic motion between the liquid and the crystal is also quite apparent in the power spectrum and in particular in the low-frequency modes. At 10 K, the power spectrum drops to zero at zero frequency. The liquid systems at 273 and more evidently at 298 K, exhibit nonzero values of the power spectrum at zero frequency. This observation is in accord with a diffusive ionic

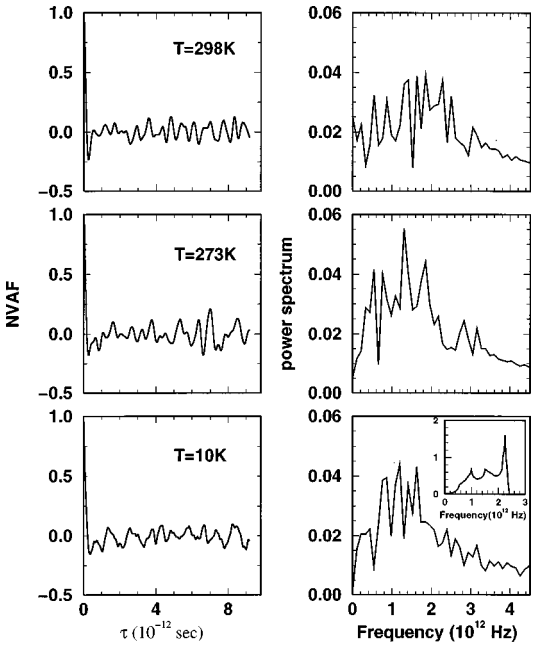

FIG. 7. Normalized velocity autocorrelation function (NVAF) and associated power spectrum for crystalline potassium ($T=10$ K) and liquid metal ($T=273,298$ K). The inset in the $T=10$ K power spectrum is the experimentally deduced phonon density of states at 9 K of Ref. 5.

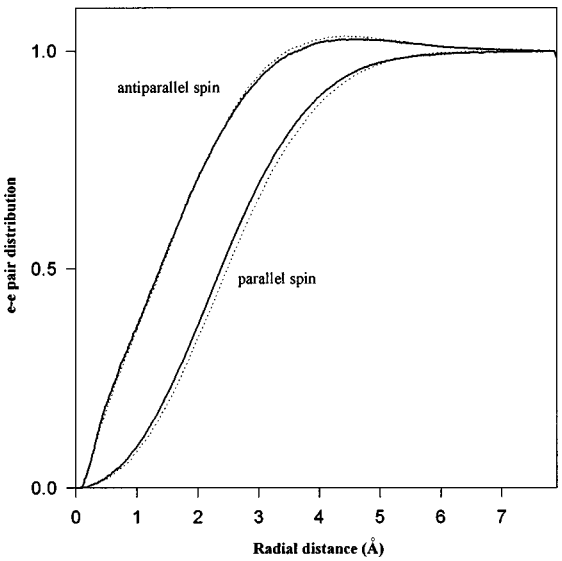

FIG. 8. Partial electron pair-correlation functions. The solid line and dotted line refer to the crystal at $T=10$ K and the liquid at 273 K, respectively.

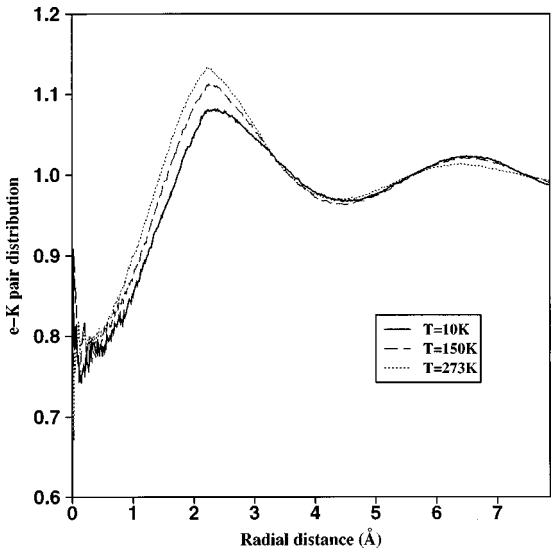

FIG. 9. Electron-ion pair-distribution functions at several temperatures.

motion.[30] The peaks in the power spectra of the liquid metal are consequences of the oscillations in the NVAF's and may thus be regarded as remnants of the phonon structure observed in the crystal state. The fact that the density of the liquid is constrained to that of the crystal may accentuate this effect. As temperature increases or density decreases, these peaks should disappear with the decay of the oscillations. It is not possible to extract detailed information from the fine structure of the power spectra because of the finite time used in their calculation. However, one may compare qualitatively the calculated power spectrum at 10 K with that deduced from experimental measurements at 9 K.[5] The experimental phonon density of states possesses a major peak near 2.1×10^{12} Hz. Vibrations in the PIMD model of the crystal potassium have lower frequencies in the range $0.8-1.3 \times 10^{12}$ Hz suggestive of weaker bonds. This observation correlates closely with the observation of a calculated melting temperature underestimating the experimental melting point.

Finally, we consider the change in the electronic structure of the metal upon melting. This change is associated with an increase in electronic kinetic energy of approximately 0.02 eV/electron. This energy is small and thus one expects only a slight modification of the electronic structure. Such a variation is observable in the electron pair-distribution functions of Fig. 8. The partial distribution functions show that the major difference between the low-temperature crystal and the liquid is an increase of the maximum in the heterospin pair correlation between 3 and 4 Å and an expansion of the exchange-correlation hole as seen in the isospin distribution. In a previous study of the effect of temperature on the electron density in an electron plasma with density near that of the present potassium system, we had shown that increasing temperature shrinks the exchange-correlation hole.[2] However, the direct effect of temperature on the electronic structure cannot be a factor as it is maintained constant by a thermostat. Here, the expansion in the parallel-spin electron correlation may thus simply be a result of volume expansion. On the other hand, upon melting the first-nearest-neighbor and second-nearest-neighbor shells of the crystal structure collapse and the ion coordination number in the liquid increases. The exchange-correlation force between neighboring isospin electrons may then induce further localization. The resulting localization within and at the border of the ionic core is seen best in the electron-ion radial distribution of Fig. 9. At low temperature the ion-electron pair distribution shows a significant first maximum at a distance of 2.2 Å. This distance corresponds to approximately one half the first-nearest-neighbor interatomic distance. The ion-electron correlation reaches a minimum between 4.3 and 4.5 Å followed by a second maximum near 6.5 Å. The ion-electron pair distribution is therefore complementary of the ion-ion distribution. In other words, high electron-ion correlation is expected where there is low ion-ion correlation. The high electron density between ions is indicative of bonding. Considering now the midpoints between ionic sites as consisting of electronic sites, we can estimate the electron-electron distance in the potassium body-centered-cubic structure to be on the order of $1/\sqrt{2}$ times the lattice parameter. The electron-electron distance thus calculated amounts to approximately 3.67 Å. This number is in excellent accord with the observed maximum in the heterospin electron-electron pair distribution. With this information, we may construct a simplified picture of the electronic structure in the crystal phase. The electron density is the highest between the ions thus leading to bonding and the electronic sites are occupied alternatively by electrons with differing spin.

An increase in electron localization at the electron sites occurs even in the solid state at the higher temperature of 150 K. This shows that atomic vibrations have a significant effect on the nature of the electronic states in crystalline potassium. Vibrations tend to localize the electron density. Similar observations by other investigators were made for the case of sodium clusters.[14] The electron density localizes further with disordering of the structure at even higher temperature. In the liquid, the electron density increases near 2.2 Å. This increase is compensated by a reduction in the electron-ion pair correlation at longer range as seen by the loss of electron-ion correlation near 6.5 Å. Since the calculated dynamical properties support the retention of vibra-

tional motion in addition to diffusive motion in the liquid state, it is unclear at this stage which of the two processes: vibration versus disorder, contributes principally to the localization. The electron localization at the edge of the ionic cores should lead to an increase in heterospin correlation between 3 and 4 Å which is observed in Fig. 8. Finally, we note that the larger electron density between nearest-neighbor ions is consistent with the shorter K-K bond length in the liquid structure.

IV. CONCLUSIONS

A first-principles molecular-dynamics scheme for the simulation of electron-ion systems with quantum-mechanical electrons modeled within the discretized path-integral formalism was applied to the study of the finite-temperature properties of a simple metal. We showed that the model potassium metal undergoes a melting transformation upon heating. The transformation is characterized thoroughly through calculated thermodynamics quantities, structural and dynamical properties. The model potassium crystal melts at a temperature significantly below the experimental melting point. The reasons for this discrepency may be found in the approximations made to speed up the calculations as, for instance, the use of a short-range interionic potential and an empty core pseudopotential. Comparison between the calculated low-temperature vibrational spectrum and the experimentally measured phonon density of states indicates that the strength of the atomic bonds is underestimated in the model. Upon melting the ionic motion changes from pure vibration to diffusive motion. Above the transition temperature, the ion mean-square displacement increases linearly with temperature; an unambiguous sign of diffusion. This change in atomic motion is also supported by the temperature dependency of the Fourier transform of the ion velocity autocorrelation function. The PIMD allows us to study the interplay between the atomic and electronic structures. In the crystalline state, vibrations appear to have an effect on the electron density and result in some electron localization. Moreover, we find that the electronic structure of the simple metal responds to the collapse in the long-range order of the ionic structure by localizing further within and at the edge of the core of the ions.

Contrary to many of the current quantum molecular-dynamics simulation techniques which rely on the independent particle approximation, the PIMD is a many-particle technique and includes the important effects of interactions of electrons with each other and with the ions. Although PIMD is a very promising technique for the study of materials in which electronic and ionic structures are intimately correlated, the shear computational cost of the algorithm constitutes a barrier to its application to large systems. At present, the restricted PIMD method is limited by the computation cost of the forces derived from the effective exchange potential. The computational cost is a quadratic function of the number of beads and a cubic function of the number of isospin electrons. Access to supercomputers can make possible the simulation of systems with larger numbers of electrons. For larger fermion systems, one may be able to optimize the calculation by exploiting the short spatial extent of exchange[31] and dividing the simulation cell into smaller and more tractable subcells. The quadratic dependency on P due to the nonlocality of the exchange potential is a more serious problem. A local effective exchange potential could lead to a linear dependency on the number of beads. We are currently developing an approximate local form of the exchange potential that is able to model the exchange interactions at a cost proportional to P only.[32] Finally, since the PIMD involves stiff oscillators, disparate masses, and short- and long-range forces, another avenue in improving the computational efficiency of our algorithm is to employ a multiple time-step scheme.[33–35]

[1] Ki-Dong Oh and P. A. Deymier, Phys. Rev. B **58**, 7577 (1998).
[2] Ki-Dong Oh and P. A. Deymier, Phys. Rev. Lett. **81**, 3104 (1998).
[3] Y. Waseda, in *The Structure of Non-Crystalline Materials* (McGraw-Hill, New York, 1980).
[4] C. B. Alcock, J. Phys. Chem. Ref. Data **23**, 385 (1994).
[5] R. A. Cowley, A. D. B. Woods, and G. Dolling, Phys. Rev. **150**, 487 (1966).
[6] W. Freyland, Phys. Rev. B **20**, 5104 (1979).
[7] W. W. Warren, Jr., in *The Metallic and Nonmetallic States of Matter*, edited by P. P. Edwards and C. N. R. Rao (Taylor & Francis, London, 1985).
[8] C. J. Smithell, *Metals Reference Handbook*, 7th ed. (Butterworth, London, 1992).
[9] R. Car and M. Parrinello, Phys. Rev. Lett. **55**, 2471 (1985).
[10] M. Parrinello, Solid State Commun. **102**, 107 (1997).
[11] R. P. Feynman and A. R. Hibbs, *Quantum Mechanics and Path Integrals* (McGraw-Hill, New York, 1965).
[12] M. Parrinello and A. Rahman, J. Chem. Phys. **80**, 860 (1984).
[13] D. Marx and M. Parrinello, Z. Phys. B **95**, 143 (1994).
[14] R. W. Hall, J. Chem. Phys. **89**, 4212 (1988); J. Phys. Chem. **93**, 5628 (1989); J. Chem. Phys. **91**, 1926 (1989).
[15] D. M. Ceperley, Phys. Rev. Lett. **69**, 331 (1992).
[16] D. M. Ceperley, Rev. Mod. Phys. **67**, 279 (1995).
[17] S. Zhang, J. Carlson, and J. E. Gubernatis, Phys. Rev. B **55**, 7464 (1997).
[18] D. Chandler and P. G. Wolynes, J. Chem. Phys. **74**, 4078 (1981).
[19] D. M. Ceperley, J. Stat. Phys. **63**, 1237 (1991).
[20] R. P. Feynman, *Statistical Mechanics* (Benjamin, New York, 1972).
[21] H. Kleinert, *Path Integral Quantum Mechanics, Statistics, and Polymer Physics* (World Scientific, Singapore, 1990).
[22] R. W. Hall, J. Chem. Phys. **93**, 8211 (1990).
[23] M. J. L. Sangster and R. M. Atwood, J. Phys. C **11**, 1541 (1978).
[24] W. A. Harrison, *Pseudopotentials in the Theory of Metals* (Benjamin, New York, 1966).
[25] R. W. Hall and B. J. Berne, J. Chem. Phys. **81**, 3641 (1984).
[26] G. J. Martyna, M. L. Klein, and M. Tuckerman, J. Chem. Phys. **97**, 2635 (1992).
[27] L. V. Woodcock, Chem. Phys. Lett. **10**, 257 (1971).
[28] M. J. Gillan, in *Computer Modelling of Fluids, Polymers and Solids*, edited by C. R. A. Catlow *et al.* (Kluwer Academic, Dordrecht, 1990), p. 155.

[29] D. A. McQuarrie, *Statistical Mechanics* (Harper and Row, New York, 1976).
[30] J. Theilhaber, Phys. Fluids B **4**, 2044 (1992).
[31] X. P. Li, R. W. Numes, and D. Vanderbilt, Phys. Rev. B **47**, 10 891 (1993).
[32] Ki-Dong Oh and P. A. Deymier (unpublished).
[33] M. E. Tuckerman, B. J. Berne, and A. Rossi, J. Chem. Phys. **94**, 1465 (1991).
[34] M. E. Tuckerman, B. J. Berne, and G. J. Martyna, J. Chem. Phys. **97**, 1990 (1992).
[35] D. A. Gibson and E. A. Carter, J. Phys. Chem. **97**, 13 429 (1993).